Industrial Chemistry & Materials

PAPER

Check for updates

Large-scale direct regeneration of LiFePO₄@C based on spray drying†

Yongxing Zou,[ab] Jinwei Cao,[ab] Hao Li,[ab] Wanbao Wu,[ab] Yihong Liang[ab] and Jiaheng Zhang (iD) *[ab]

Direct regeneration is a low-cost and environmentally friendly way of recycling spent Li-ion batteries. In this study, a new method is adopted to regenerate spent LiFePO₄. First, the spent LiFePO₄ powder is homogenized, and then, small amounts of a lithium source and a carbon source are thoroughly mixed by spray drying. After that, a high-temperature solid-phase method is used to regenerate the carbon-coated lithium iron phosphate. Compared with traditional regeneration methods, the proposed method significantly improves the universality of spent LiFePO₄ having different degrees of damage. The regenerated LiFePO₄ is characterized using X-ray diffraction, scanning electron microscopy, transmission electron microscopy, Raman spectroscopy, and electrochemical measurements. The results show that the regenerated sample has a stable morphology, structure, and electrochemical performance. Under the conditions of 0.1C, the initial capacity exceeds 160 mA h g⁻¹. After 800 cycles under the conditions of 1C, the capacity retention is 80%, which satisfies the requirements for regenerated LiFePO₄ batteries.

1 Introduction

Lithium-ion batteries (LIBs) are widely used in electronic devices owing to their high energy density and long service life. Among these, olivine lithium iron phosphate (LiFePO₄ or LFP) has the advantages of thermal stability, long cycle life, and low cost, and it is popular for use in power batteries of electric vehicles.[1] However, lithium-ion batteries have limited life spans. Generally, the life spans of these electric vehicle power batteries are 5–10 years. With the rapid development of electric vehicles, the next few years will usher in battery scrapping, which will inevitably generate a large number of end-of-life batteries.[2,3] Recycling technology and harmless treatment technology for end-of-life batteries have become topics of concern.[4–6]

Research has focused on recycling valuable metals such as Co, Ni, and Li from cathode materials using various methods, such as hydrometallurgical technology, pyrometallurgical technology, and biotechnology.[7–13] However, these processes are more suitable for waste LIBs containing the Ni and Co elements, such as LCO-, NCM-, and

NCA-type, and are not applicable to waste LIBs without the Ni and Co elements, such as LFP- and LMO-type.[14–16] Moreover, these recycling processes also have some obvious disadvantages: (a) the use of a large amount of chemical reagents, which is very likely to cause secondary pollution and generate a large amount of waste water and waste gas; (b) the process is long, and the cost of repair and regeneration is too high, thus compromising the practical application value.[17–19] In contrast, direct regeneration of spent LFP is a more environmentally friendly method with practical application value.

Common regeneration methods are mainly hydrothermal and solid-phase regeneration.[20–25] Hydrothermal regeneration mainly involves the repair of spent LFP by adding a specific proportion of a lithium source and a reducing agent. Xu *et al.*[26] reported a low-temperature aqueous solution repair method for LiFePO₄ using LiOH and citric acid as the lithium source and the reducing agent, respectively; the reaction was carried out at 60–180 °C for a certain time, followed by rapid annealing at 600 °C for 2 h. The electrochemical properties of the regenerated product were similar to those of commercial LiFePO₄. Song *et al.*[27] mixed LiFePO₄ scraps with graphene oxide, added a lithium source and a reducing agent, and reduced graphene oxide while replenishing lithium in the hydrothermal liquid phase to obtain homogeneous and fine nanosphere composites. Solid-phase regeneration was mainly achieved by adding a lithium source (LiOH, Li₂CO₃) and a carbon source (glucose, lecithin, sucrose, and polyvinyl alcohol)

[a] Sauvage Laboratory for Smart Materials, Harbin Institute of Technology (Shenzhen), Shenzhen, 518055, China. E-mail: zhangjiaheng@hit.edu.cn
[b] Research Centre of Printed Flexible Electronics, School of Materials Science and Engineering, Harbin Institute of Technology (Shenzhen), Shenzhen, 518055, China
† Electronic supplementary information (ESI) available. See DOI: https://doi.org/10.1039/d2im00007e

to rehabilitate spent LFP by high-temperature roasting. Li et al.[28] sintered recycled a cathode material with Li_2CO_3 and sucrose to regenerate new $LiFePO_4/C$ materials. The effect of Li_2CO_3 addition on the performance of the resynthesized $LiFePO_4/C$ material was investigated. The performance improved when the added amount of Li_2CO_3 was 1.4 wt%; the discharge capacity was 142.75 mA h g^{-1} in the first cycle at 0.2C conditions, and the retention rate was 95.32% after 100 cycles.

These repair and regeneration methods are helpful for the repair of spent $LiFePO_4$; however, they have some shortcomings. The electrochemical properties of the regenerated samples under the same regeneration conditions can be inconsistent because the spent $LiFePO_4$ could have been damaged to different degrees. This will limit the large-scale applications of the regenerated $LiFePO_4$. Moreover, there are still some impurities in spent $LiFePO_4$, such as residual electrolytes and binder, which hamper the formation of uniform and stable regenerated $LiFePO_4$.[29] The reported capacity values of the regenerated samples are relatively low, and it is challenging to achieve a comparable capacity to that of the unused $LiFePO_4$.

To overcome the abovementioned challenges, we developed a closed-loop, scalable LIB recovery process that incorporates homogenization treatment, spray drying, and carbon thermal reduction (Fig. 1). The regenerated cathode material demonstrated excellent electrochemical performance, similar to that of commercial $LiFePO_4$, especially under low rate conditions. The regeneration process is rapid, stable, and scalable. The specific process is as follows: (1) the spent lithium iron phosphate (S-LFP) battery cathode material was sintered at a high temperature in an air atmosphere to remove impurities and achieve homogenization; a red material primarily comprising Fe_2O_3 and $Li_3Fe_2(PO_4)_3$ was obtained. (2) The homogenized lithium iron phosphate (Homo-LFP) was mixed with Li_2CO_3 (lithium source), and ascorbic acid (reducing agent, carbon source) in deionized water. The mixed solution was placed in a ball mill and mixed thoroughly to obtain a spray-drying precursor solution. (3) The solution was spray-dried, and the resulting mixture was sintered in an Ar atmosphere, and a black powder was obtained. The black powder was rinsed with deionized water to remove water-soluble by-products; thus, carbon-coated lithium iron phosphate was obtained. The regenerated lithium iron phosphate (R-LFP) material exhibited excellent physical and electrochemical properties, and can meet the reuse requirements of commercial LFP batteries. This economical method has good application prospects.

2 Results and discussion

2.1 Characterization of control and regenerated cathode materials

Inductively coupled plasma optical emission spectrometry (ICP-OES), and a carbon and sulfur analyzer were used to detect the elemental content of each sample. The major
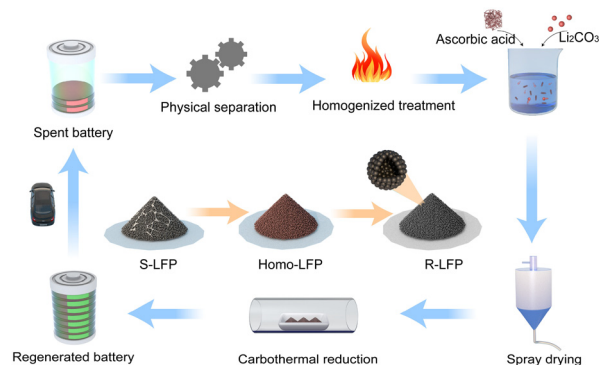

Fig. 1 Schematic illustration of the regeneration process of spent LFP.

elemental compositions of S-LFP, Homo-LFP, and R-LFP are shown in Table 1. S-LFP contained approximately 4.41 wt% Li, 34.53 wt% Fe, 15.58 wt% P, and 1.38 wt% C. The molar ratio of Li : Fe is 1.02 : 1, which is slightly greater than 1. This could result from the over-discharge of the used battery before dismantling and some of the lithium-containing electrolytes remaining in the cathode powder. For R-LFP, approximately 4.47 wt% was Li, 31.29 wt% was Fe, 14.87 wt% was P, and 7.38 wt% was C. The molar ratio of Li : Fe : P was 1.09 : 1 : 0.98. A small amount of lithium source was added to ensure that lithium is correctly positioned in the regenerated LFP and to reduce Li–Fe "anti-site" pairs.[30] The regeneration process increases the Li–Fe ratio from 1.02 to 1.09 and the carbon content from 1.31 to 7.38 wt%, which facilitates the reduction of Li–Fe anti-sites and achieves carbon encapsulation of LFP.

The crystalline structure of S-LFP was analyzed by X-ray diffraction (XRD), as shown in Fig. 2a. Though the diffraction peaks of the discarded S-LFP powder are dominated by olivine LFP (JCPDS 81-1173), the impurity peaks near $2\theta = 22.3°$ and $2\theta = 23°$ are non-negligible. Fig. 2b shows the XRD patterns of Homo-LFP and R-LFP. The homogenized sample mainly comprised Fe_2O_3 (JCPDS 89-0597) and $Li_3Fe_2(PO_4)_3$ (JCPDS 47-0107). The XRD spectrum of R-LFP was in good agreement with the standard PDF card (#81-1173, $LiFePO_4$). The diffraction peaks are sharp and clear, and no other phases or impurities can be observed, which indicates that the regeneration process could effectively restore the crystalline structure of LFP.

Fig. 2c shows the scanning electron microscopy (SEM) images of spent $LiFePO_4$. The morphology of the spent sample was irregular, showing more agglomerates and even a tiny amount of incompletely decomposed PVDF binder. The agglomerates and residual PVDF could hinder Li^+ transport during charging and discharging, which would reduce the

Table 1 The major element content of the samples

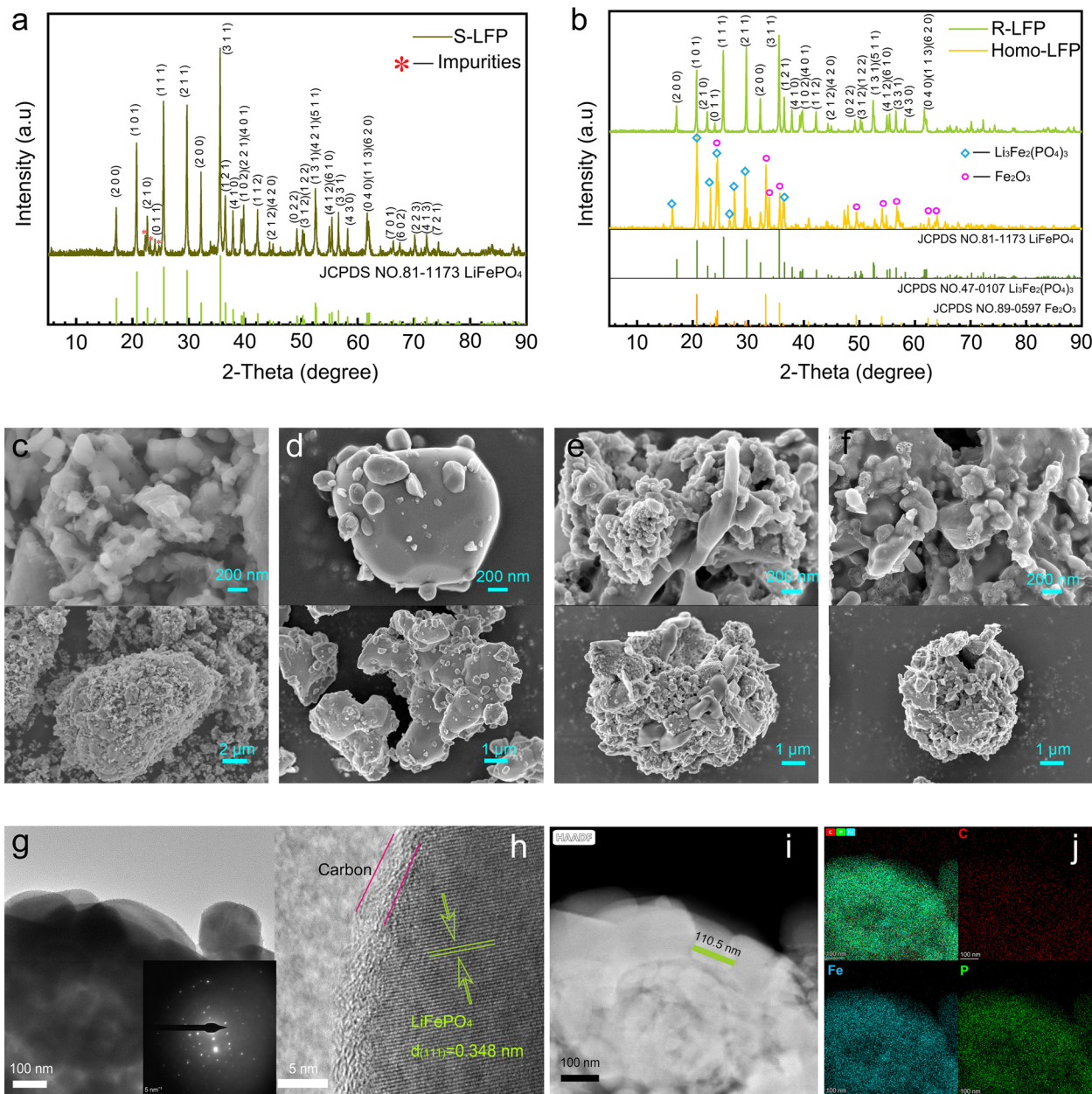| Mass ratio/%	Fe	Li	P	C
S-LFP	34.53%	4.41%	15.58%	1.31%
Homo-LFP	31.29%	4.47%	16.38%	~0
R-LFP	27.39%	3.74%	14.87%	7.38%

Fig. 2 Phase analysis and morphological characterization of samples. XRD patterns of (a) S-LFP, (b) Homo-LFP and R-LFP; SEM images of (c) S-LFP, (d) Homo-LFP, (e) spray-dried LFP and (f) R-LFP; (g and h) TEM images of R-LFP; (i and j) HAADF-STEM image and EDS elemental mappings of R-LFP.

electrochemical performance.[31] Fig. 2d shows the SEM images of samples after the homogenization treatment, where the large agglomerates disappeared and the PVDF binder was eliminated. Fig. 2e shows the microscopic morphology after spray drying, and it can be observed that the secondary particles exhibited hollow-sphere-like structures. Fig. 2f shows the microscopic morphology of the R-LFP sample, which maintains a hollow spherical shell secondary structure.

High-resolution TEM (HR-TEM) was used to observe the morphologies of the regenerated sample. Fig. 2g and h show that the microstructure of R-LFP was regular with high

crystallinity, and the measured layer spacing was 0.348 nm, which corresponded to the (111) crystal plane of $LiFePO_4$. A coating layer of 3 nm can be observed at the particle surface, which is attributed to a layer of carbon coating. Carbon coating on the surface helps to improve the electrochemical properties and prevent excessive grain growth. Fig. 2i shows the HAADF-STEM image of R-LFP, where elliptical grains with a long axis of approximately 110.5 nm can be distinguished. The energy dispersive X-ray spectroscopy (EDXS) mappings of the main elements C, Fe, and P for R-LFP are shown in Fig. 2j, which indicates the uniform element distribution throughout the sample.
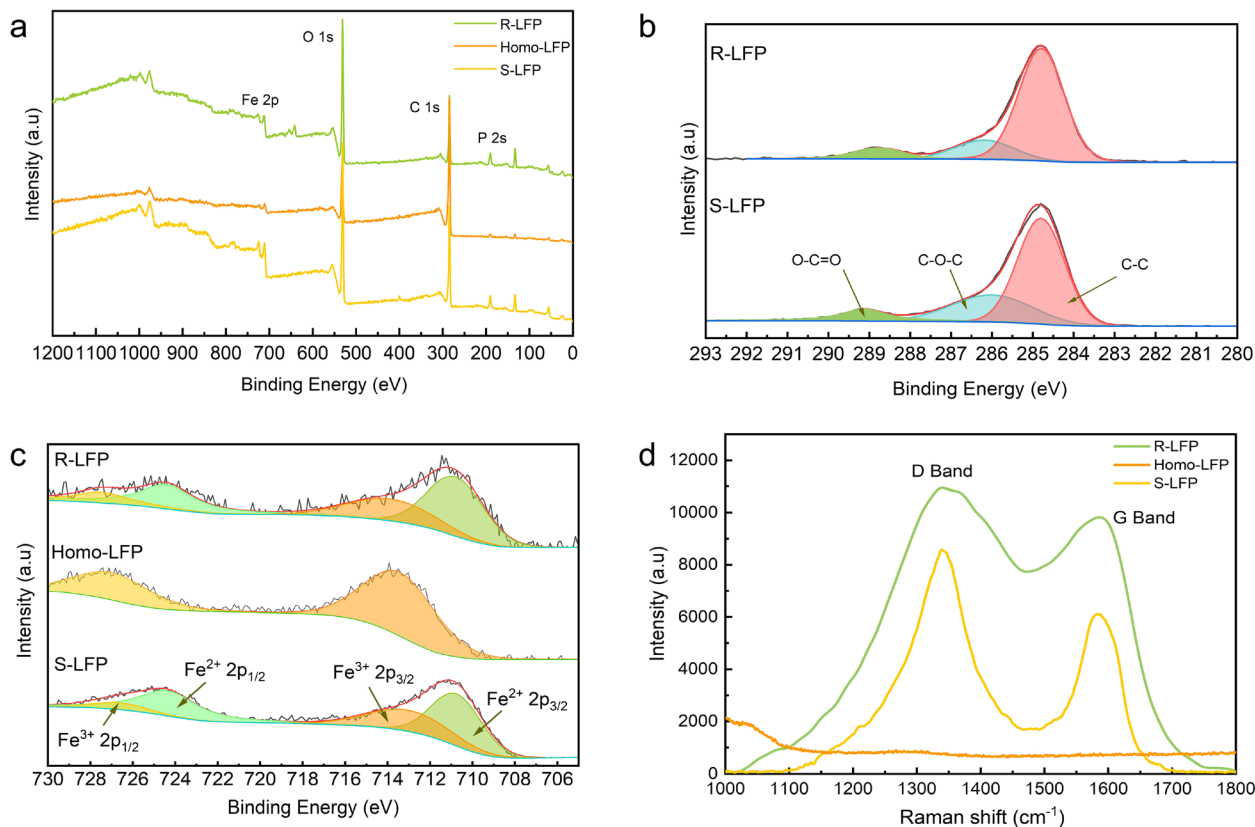
Fig. 3 XPS and Raman spectra of the samples. (a) XPS survey spectra for the samples; high-resolution spectra of (b) C 1s and (c) Fe 2p; (d) Raman spectra of the samples.

Surface analysis of S-LFP, Homo-LFP, and R-LFP was carried out using X-ray photoelectron spectroscopy (XPS). As shown in Fig. 3a, the XPS survey spectra of S-LFP, Homo-LFP, and R-LFP clearly show the elemental peaks of P 2s, C 1s, O 1s, and Fe 2p. The calibration of all the sample peaks was conducted with respect to the C 1s species. In S-LFP and R-LFP, the signal of C 1s is deconvoluted into three peaks, at binding energies of 284.8 eV (C–C), 286 eV (C–O–C), and 288.5 eV (O–C=O).[32] The distribution of the types of C species in the samples is illustrated in Fig. 3b. The ratio of C–O–C to C–C in S-LFP could be determined from the XPS result, which is 0.44. On the other hand, in R-LFP, this ratio is 0.21, which shows that R-LFP has fewer defects in the carbon layer. Similarly, the signal of Fe 2p is deconvoluted into four peaks.[33] The distribution of Fe in the samples is illustrated in Fig. 3c. XPS revealed that the ratio of Fe^{3+} to Fe^{2+} was 0.67 in S-LFP and 0.53 in R-LFP, indicating that there were fewer Fe^{3+} impurities in the regenerated samples.

The presence of carbon in the samples was further characterized by Raman spectroscopy. The Raman spectra of the samples are listed in Table 2. D-band and G-band peaks were observed at ~1360 cm^{-1} and ~1560 cm^{-1}, respectively, representing the lattice defects and the in-plane stretching vibration of the sp^2 hybridized C atoms.[34] Comparing the I_D/I_G (intensity ratio of the D-band to the G-band) of the samples, it is observed that the I_D/I_G of the regenerated

samples is much smaller than that of the spent LFP. This indicates a higher degree of graphitization of the carbon cladding layer in the regenerated LFP. The higher degree of graphitization is beneficial to improve the electrical conductivity and thus to improve the charge/discharge performance of the regenerated samples. The absence of the D-band and G-band in the homogenized LFP indicated that the residual carbon in the spent LFP was sufficiently removed, and the regenerated sample was not affected by the residual PVDF and organic electrolyte, which significantly improves the stability of the regeneration.

2.2 Electrochemical performances of spent and regenerated LiFePO₄

The first four cycles of voltammetry results for the spent and regenerated LFP are shown in Fig. 4a and b, respectively. They comprise a pair of anode and cathode peaks, representing the charge–discharge reaction. The regenerated

Table 2 Raman data of the samples

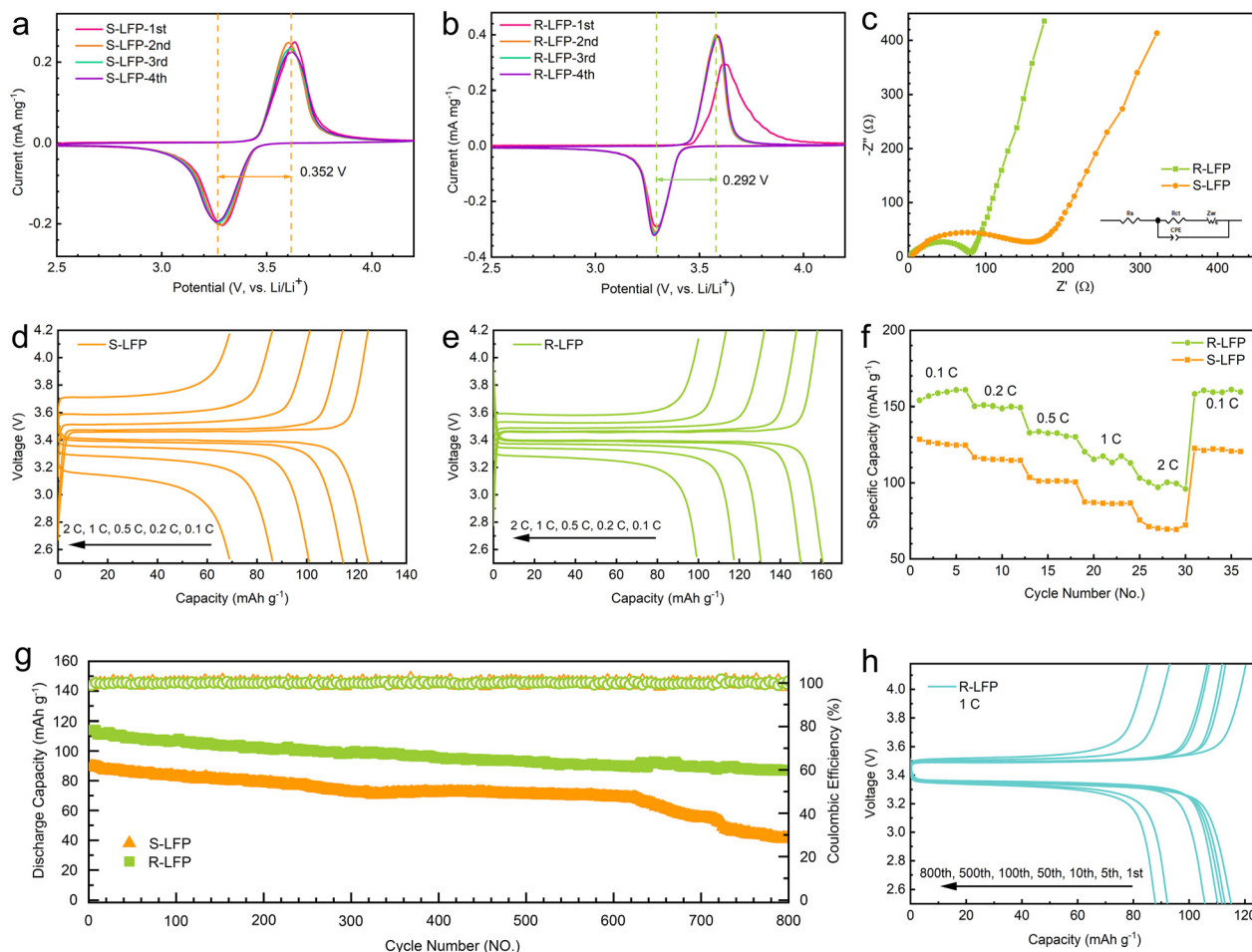| Sample	I_D	I_G	I_D/I_G
S-LFP	8579.22	6106.80	1.4049
Homo-LFP	No peak	No peak	—
R-LFP	10 938.50	9818.90	1.1140

Fig. 4 Electrochemical performances of S-LFP and R-LFP. CV curves of (a) S-LFP and (b) R-LFP; (c) Nyquist plots of R-LFP and S-LFP; charge–discharge curves of (d) S-LFP and (e) R-LFP at different rates; (f) rate performance of samples; (g) long-term cycling stability of S-LFP and R-LFP; (h) charge–discharge curves of R-LFP after several cycles.

LFP had a small potential difference (0.292 V) between the two redox reactions, which was significantly smaller than that of the spent LFP (0.352 V). This indicates that the cell containing regenerated LFP had a lower polarization. In the subsequent cycles, the peak position and the intensity of R-LFP remained stable, which indicates the high reversibility of the regenerated sample. This suggests that the cyclic performance of the regenerated sample was much better than that of the spent LFP.

To further understand the electrochemical performance of the regenerated samples, EIS measurements were performed in the frequency range of 100 kHz–0.05 Hz with an uptake amplitude of 10 mV. Fig. 4c shows the Nyquist plots of the spent and regenerated LFP samples. The EIS spectrum comprised a depressed semicircle in the high-frequency region and a straight line in the low-frequency region. In general, the total resistance (R_s) of the electrolyte and electrode material was the intercept of the semicircle in the high-frequency region, and the charge-transfer resistance (R_{ct}) was the semicircle diameter.[35] The corresponding R_s and R_{ct} values (as listed in Table 3) could be obtained by fitting

the EIS curves with an equivalent circuit model. Table 3 shows that the regenerated sample had smaller R_s and R_{ct} values. The results indicate that the EIS performance of the regenerated sample was superior because of the improved particle structure, good carbon encapsulation, and low impurity content.[36]

The charging and discharging curves of spent LFP and regenerated LFP at different rates are shown in Fig. 4d and e; the discharge capacities of S-LFP were 124.6, 114.2, 100.7, 86.8, and 70.0 mA h g^{-1} at discharge rates of 0.1, 0.2, 0.5, 1, and 2C, respectively. Meanwhile, the discharge capacities of R-LFP were 160.8, 150.0, 130.6, 117.3, and 100.1 mA h g^{-1} at discharge rates of 0.1, 0.2, 0.5, 1, and 2C, respectively. The charge/discharge specific capacity of the regenerated LiFePO$_4$ was better than that of the spent LiFePO$_4$ sample.

Table 3 Equivalent circuit parameter fitting based on experimental data

Sample	R_s (Ω)	R_{ct} (Ω)
Spent LFP	4.378	131.7
Regenerated LFP	1.866	81.61

As shown in Fig. 4f, the rate performance of each sample exhibited a clear stepwise trend. The discharge capacities of the regenerated LFP at 0.1, 0.2, 0.5, 1, and 2C were ~160, ~150, ~135, ~120, and ~100 mA h g^{-1}, respectively, which are much better than those of the spent LFP. The cycling performance of the regenerated LiFePO$_4$ and spent LiFePO$_4$ at 1C rate is shown in Fig. 4g. After 600 cycles, the discharge performance of the spent LFP decreased significantly. The regenerated LFP maintained approximately 80% capacity after 800 cycles, and the coulombic efficiency was steadily maintained near 100%. The charging and discharging curves of R-LFP after several cycles are shown in Fig. 4h, and the voltage of the charging and the discharging platform remains stable during the cycle. The discharge capacities of the regenerated LFP at the 1st, 5th, 10th, 50th, 100th, 500th, and 800th turns were 115.1, 112.9, 111.8, 110.3, 115.7, 92.2, and 87.9 mA h g^{-1}, respectively. The regenerated LiFePO$_4$ exhibited excellent cycling performance and was capable of meeting industrial recycling requirements.

In addition, the regeneration of 1 ton lithium iron phosphate by this method requires 1 ton of S-LFP black powder, 0.01 tons of lithium carbonate, and 0.07 tons of glucose. The cost of these materials is ¥72 339 per ton, which is 51.02% that of the raw material lithium iron phosphate (please see the ESI† for assessment details). The cost of regeneration is significantly lower than the market price of lithium iron phosphate and provides a basis for industrial production.

3 Conclusion

In this study, a scalable and closed-loop lithium-ion battery recycling process is proposed. The process includes homogenization, spray drying, and carbon thermal reduction. Regenerated LiFePO$_4$@C shows a restored lattice structure, uniform surface carbon coating, and excellent electrochemical properties. In this work, the regenerated LiFePO$_4$ shows a capacity of more than 160 mA h g^{-1} at 0.1 C and maintained approximately 80% of the initial capacity value at a 1C rate for 800 cycles. The regenerated LiFePO$_4$ had stable performance, and the regeneration method was simple and resource-saving, showing great potential for application to the recycling industry.

4 Experimental procedures

4.1 Sample preparation

Spent LFP was provided in large quantities by a local professional power battery recycling company (Shenzhen Hengchuang Ruineng Environmental Technology Co. Ltd.). Super P, polyvinylidene fluoride (PVDF), *N*-methylpyrrolidone (NMP), LiPF$_6$, dimethyl carbonate (DMC), and ethylene carbonate (EC) were provided by Guangdong Canrd New Energy Technology Co., Ltd.

To remove impurities in the spent LFP powder and homogenize the composition, 50 g of spent LFP was weighed into a porcelain boat and placed in a muffle furnace at 800 °C for 150 min. This step helps to sufficiently remove the remaining electrolyte, adhesive, carbon black, and other impurities.

4.2 Spray drying and sintering to obtain regenerated LFP

The process mainly consists of precursor preparation, spray drying, and roasting. An appropriate amount of the sample was taken after the aforementioned treatment to prepare an aqueous solution. Li$_2$CO$_3$ (1 wt%), ascorbic acid (30 wt%), a small amount of graphene, and sodium dodecylbenzene sulfonate were added as surfactants, and all the components were mixed thoroughly by wet ball milling. In this experiment, 10 g of lithium iron phosphate, 0.1 g of Li$_2$CO$_3$, 3 g of ascorbic acid, and 0.1 g of sodium dodecylbenzene sulfonate were mixed in 100 mL of deionized water, and then wet ball milled at 280 rpm for 10 h. After spray drying of the precursor solution, 4 g of the spray-dried product was placed in a porcelain boat and roasted at 350 °C for 4 h under an atmosphere containing Ar to obtain a black powder; then, this powder was heated to 650 °C for 10 h at a rate of 3 °C min^{-1}. The black powder was rinsed with deionized water to remove water-soluble by-products and dried under vacuum at 80 °C for 24 h to obtain the carbon-coated LFP.

4.3 Characterization of the composition and structure of the sample

The elemental composition of the sample was determined using inductively coupled plasma optical emission spectrometry (ICP-OES, Agilent 720ES). The phase composition was determined using X-ray diffraction (XRD, Rigaku Ultima VI Type), and the morphology was examined using scanning electron microscopy (SEM, Zeiss Sigma300). X-ray photoelectron spectroscopy (XPS, KRATOS AXIS Ultra DLD) was used to characterize the valence states of Fe and C on the sample surface. Raman spectroscopy (Horiba Scientific LabRAM HR Evolution) was used to characterize the carbon coatings on the surfaces. Transmission electron microscopy (TEM, FEI Talos F200X) was used to observe the thickness of the carbon coating and the lattice spacings.

4.4 Electrochemical performance of regenerated LFP

The cathode was prepared by coating a slurry containing 80% active material, 10% Super P, and 10% PVDF. After the addition of NMP, the slurry was stirred for 12 h. The slurry was coated on an aluminum foil substrate and then vacuum-dried at 80 °C for 12 h.

The amount of active material was approximately 1.5 mg cm^{-2}. Electrochemical measurements were performed at 25 °C using a CR2032 coin-type battery with lithium as the anode. A DMC–EC mixed solvent containing 1.0 M LiPF$_6$ and 5% FEC was used as the electrolyte. The battery was assembled in a glove box filled with argon, and the H$_2$O and O$_2$ contents were <0.1 ppm. A Neware instrument was used to study the

© 2023 The Author(s). Co-published by the Institute of Process Engineering, Chinese Academy of Sciences and the Royal Society of Chemistry

Ind. Chem. Mater., 2023, **1**, 254–261 | **259**

constant current charge and discharge capacity and rate performance at different current densities in the voltage range of 2.5–4.2 V. Cyclic voltammetry (CV) tests were performed on a CHI 760E (CH, Shanghai, China) electrochemical workstation with voltages of 2.5 and 4.2 V, and a scan rate of 0.01 mV s^{-1}. For electrochemical impedance spectroscopy (EIS), the frequency range was selected from 100 kHz to 0.05 Hz, and the amplitude was 10 mV.

Conflicts of interest

The authors declare no conflict of interest.

Acknowledgements

References

1 B. S. Dunn, H. Kamath and J. M. Tarascon, Electrical Energy Storage for the Grid: A Battery of Choices, *Science*, 2011, **334**, 928–935.

2 W. Wang and Y. Wu, An Overview of Recycling and Treatment of Spent LiFePO$_4$ Batteries in China, *Resour., Conserv. Recycl.*, 2017, **127**, 233–243.

3 T. Or, S. W. D. Gourley, K. Kaliyappan, A. Yu and Z. Chen, Recycling of Mixed Cathode Lithium-Ion Batteries for Electric Vehicles: Current Status and Future Outlook, *Carbon Energy*, 2020, **2**, 6–43.

4 K. Du, E. H. Ang, X. Wu and Y. Liu, Progresses in Sustainable Recycling Technology of Spent Lithium-Ion Batteries, *Energy Environ. Mater.*, 2021, 1012–1036.

5 R. Bird, Z. J. Baum, X. Yu and J. Ma, The Regulatory Environment for Lithium-Ion Battery Recycling, *ACS Energy Lett.*, 2022, **7**, 736–740.

6 E. Fan, L. Li, Z. Wang, J. Lin, Y. Huang, Y. Yao, R. Chen and F. Wu, Sustainable Recycling Technology for Li-Ion Batteries and Beyond: Challenges and Future Prospects, *Chem. Rev.*, 2020, **120**, 7020–7063.

7 P. Moazzam, Y. Boroumand, P. Rabiei, S. S. Baghbaderani, P. Mokarian, F. Mohagheghian, L. J. Mohammed and A. Razmjou, Lithium Bioleaching: An Emerging Approach for the Recovery of Li from Spent Lithium Ion Batteries, *Chemosphere*, 2021, **277**, 130196.

8 J. Ordoñez, E. J. Gago and A. Girard, Processes and Technologies for the Recycling and Recovery of Spent Lithium-Ion Batteries, *Renewable Sustainable Energy Rev.*, 2016, **60**, 195–205.

9 X. Wang, X. Wang, R. Zhang, Y. Wang and H. Shu, Hydrothermal Preparation and Performance of LiFePO$_4$ by using Li$_3$PO$_4$ Recovered from Spent Cathode Scraps as Li Source, *Waste Manage.*, 2018, **78**, 208–216.

10 E. M. S. Barbieri, E. P. C. Lima, S. J. Cantarino, M. F. F. Lelis and M. B. J. G. Freitas, Recycling of Spent Ion-Lithium Batteries as Cobalt Hydroxide, and Cobalt Oxide Films Formed under a Conductive Glass Substrate, and Their Electrochemical Properties, *J. Power Sources*, 2014, **269**, 158–163.

11 M. Joulié, R. Laucournet and E. Billy, Hydrometallurgical Process for the Recovery of High Value Metals from Spent Lithium Nickel Cobalt Aluminum Oxide based Lithium-Ion Batteries, *J. Power Sources*, 2014, **247**, 551–555.

12 D. Song, X. Wang, H. Nie, H. Shi, D. Wang, F. Guo, X. Shi and L. Zhang, Heat Treatment of LiCoO$_2$ Recovered from Cathode Scraps with Solvent Method, *J. Power Sources*, 2014, **249**, 137–141.

13 L. Yang, G. Xi and Y. Xi, Recovery of Co, Mn, Ni, and Li from Spent Lithium Ion Batteries for the Preparation of LiNi$_x$Co$_y$Mn$_z$O$_2$ Cathode Materials, *Ceram. Int.*, 2015, **41**, 11498–11503.

14 M. Wang, K. Liu, S. Dutta, D. S. Alessi, J. Rinklebe, Y. S. Ok and D. C. W. Tsang, Recycling of Lithium Iron Phosphate Batteries: Status, Technologies, Challenges, and Prospects, *Renewable Sustainable Energy Rev.*, 2022, **163**, 112515.

15 X. Chen, Y. Wang, S. Li, Y. Jiang, Y. Cao and X. Ma, Selective Recycling of Valuable Metals from Waste LiCoO$_2$ Cathode Material of Spent Lithium-Ion Batteries through Low-Temperature Thermochemistry, *Chem. Eng. J.*, 2022, **434**, 134542.

16 M. K. Tran, M.-T. F. Rodrigues, K. Kato, G. Babu and P. M. Ajayan, Deep Eutectic Solvents for Cathode Recycling of Li-ion Batteries, *Nat. Energy*, 2019, **4**, 339–345.

17 G. Harper, R. Sommerville, E. Kendrick, L. Driscoll, P. Slater, R. Stolkin, A. Walton, P. Christensen, O. Heidrich, S. Lambert, A. Abbott, K. Ryder, L. Gaines and P. Anderson, Recycling Lithium-ion Batteries from Electric Vehicles, *Nature*, 2019, **575**, 75–86.

18 R. E. Ciez and J. F. Whitacre, Examining Different Recycling Processes for Lithium-Ion Batteries, *Nat. Sustain.*, 2019, **2**, 148–156.

19 Y. Yao, M. Zhu, Z. Zhao, B. Tong, Y. Fan and Z. Hua, Hydrometallurgical Processes for Recycling Spent Lithium-Ion Batteries: A Critical Review, *ACS Sustainable Chem. Eng.*, 2018, **6**, 13611–13627.

20 X. Song, T. Hu, C. Liang, H. L. Long, L. Zhou, W. Song, L. You, Z. S. Wu and J. W. Liu, Direct Regeneration of Cathode Materials from Spent Lithium Iron Phosphate Batteries using a Solid Phase Sintering Method, *RSC Adv.*, 2017, **7**, 4783–4790.

21 L. Wang, J. Li, H. Zhou, Z. Huang, S. Tao, B. Zhai, L. Liu and L. Hu, Regeneration Cathode Material mixture from Spent Lithium Iron Phosphate Batteries, *J. Mater. Sci.: Mater. Electron.*, 2018, **29**, 9283–9290.

22 J. Chen, Q. Li, J. Song, D. Song, L. Zhang and X. Shi, Environmentally Friendly Recycling and Effective Repairing of Cathode Powders from Spent LiFePO$_4$ Batteries, *Green Chem.*, 2016, **18**, 2500–2506.

23 Y. Zhao, X. Yuan, L. Jiang, J. Wen, H. Wang, R. Guan, J. Zhang and G. Zeng, Regeneration and Reutilization of

Cathode Materials from Spent Lithium-Ion Batteries, *Chem. Eng. J.*, 2020, **383**, 123089.

24 Y. Song, B. Xie, S. Song, S. Lei, W. Sun, R. Xu and Y. Yang, Regeneration of LiFePO$_4$ from Spent Lithium-Ion Batteries via a Facile Process Featuring Acid Leaching and Hydrothermal Synthesis, *Green Chem.*, 2021, **23**, 3963–3971.

25 J. Kumar, R. R. Neiber, J. Park, R. Ali Soomro, G. W. Greene, S. Ali Mazari, H. Young Seo, J. Hong Lee, M. Shon, D. Wook Chang and K. Yong Cho, Recent Progress in Sustainable Recycling of LiFePO$_4$-Type Lithium-Ion Batteries: Strategies for Highly Selective Lithium Recovery, *Chem. Eng. J.*, 2022, **431**, 133993.

26 P. Xu, Q. Dai, H. Gao, H. Liu, M. Zhang, M. Li, Y. Chen, K. An, Y. S. Meng, P. Liu, Y. Li, J. S. Spangenberger, L. Gaines, J. Lu and Z. Chen, Efficient Direct Recycling of Lithium-Ion Battery Cathodes by Targeted Healing, *Joule*, 2020, **4**, 2609–2626.

27 W. Song, J. Liu, L. You, S. Wang, Q. Zhou, Y. Gao, R. Yin, W. Xu and Z. Guo, Re-synthesis of Nano-Structured LiFePO$_4$/Graphene Composite Derived from Spent Lithium-Ion Battery for Booming Electric Vehicle Application, *J. Power Sources*, 2019, **419**, 192–202.

28 X. Li, J. Zhang, D. Song, J. Song and L. Zhang, Direct Regeneration of Recycled Cathode Material Mixture from Scrapped LiFePO$_4$ Batteries, *J. Power Sources*, 2017, **345**, 78–84.

29 Q. Sun, X. Li, H. Zhang, D. Song, X. Shi, J. Song, C. Li and L. Zhang, Resynthesizing LiFePO$_4$/C Materials from the Recycled Cathode via a Green Full-Solid Route, *J. Alloys Compd.*, 2020, **818**, 153292.

30 M. S. Islam, D. J. Driscoll, C. A. J. Fisher and P. R. Slater, Atomic-Scale Investigation of Defects, Dopants, and Lithium Transport in the LiFePO$_4$ Olivine-Type Battery Material, *Chem. Mater.*, 2005, **17**, 5085–5092.

31 L. Guan, M. Liu, F. Yu, T. Qiu, T. Zhou and X. Lin, A LiFePO$_4$ Regeneration Method based on PVAc Alcoholysis Reaction, *Renewable Energy*, 2021, **175**, 559–567.

32 A. V. Shchukarev and D. V. Korolkov, XPS Study of Group IA Carbonates, *Cent. Eur. J. Chem.*, 2004, **2**, 347–362.

33 M. C. Biesinger, B. P. Payne, A. P. Grosvenor, L. W. M. Lau, A. R. Gerson and R. S. C. Smart, Resolving Surface Chemical States in XPS Analysis of First Row Transition Metals, Oxides and Hydroxides: Cr, Mn, Fe, Co and Ni, *Appl. Surf. Sci.*, 2011, **257**, 2717–2730.

34 M. A. Pimenta, G. Dresselhaus, M. S. Dresselhaus, L. G. Cancado, A. Jorio and R. Saito, Studying Disorder in Graphite-Based Systems by Raman Spectroscopy, *Phys. Chem. Chem. Phys.*, 2007, **9**, 1276–1291.

35 M. Gaberscek, J. Moskon, B. Erjavec, R. Dominko and J. Jamnik, The Importance of Interphase Contacts in Li Ion Electrodes: The Meaning of the High-Frequency Impedance Arc, *Electrochem. Solid-State Lett.*, 2008, **11**, A170.

36 J. Zhang, X. Li, D. Song, Y. Miao, J. Song and L. Zhang, Effective Regeneration of Anode Material Recycled from Scrapped Li-ion Batteries, *J. Power Sources*, 2018, **390**, 38–44.

© 2023 The Author(s). Co-published by the Institute of Process Engineering, Chinese Academy of Sciences and the Royal Society of Chemistry

Ind. Chem. Mater., 2023, **1**, 254–261 | **261**